Article

An Exploration of a Balanced Up-downwind Scheme for Solving Heston Volatility Model Equations on Variable Grids

Chong Sun* and **Qin Sheng**

Department of Mathematics and Center for Astrophysics, Space Physics, and Engineering Research, Baylor University, One Bear Place, Waco, TX 76798-7328, USA; chong_sun@baylor.edu; qin_sheng@baylor.edu

* Correspondence: chong_sun@baylor.edu

Version October 29, 2018 submitted to Preprints

Abstract: This paper studies an effective finite difference scheme for solving two-dimensional Heston stochastic volatility option pricing model problems. A dynamically balanced up-downwind strategy for approximating the cross-derivative is implemented and analyzed. Semi-discretized and spatially nonuniform platforms are utilized. The numerical method comprised is simple, straightforward with reliable first order overall approximations. The spectral norm is used throughout the investigation and numerical stability is proven. Simulation experiments are given to illustrate our results.

Keywords: Heston volatility model; initial-boundary value problems; finite difference approximations; up-downwind scheme; order of convergence; stability

---

1. Introduction

Demands of highly effective, efficient and reliable numerical methods have been increasingly high for solving option trading modeling equations involving cross-derivative terms. However, desirable computational procedures are in general difficult to obtain due to challenges from the participation of cross-derivatives [6,15]. This motivates our study. In this investigation, targeting at European options that can only be exercised on dates of maturity, we propose and analyze a new and dynamically balanced up-downwind finite finite difference method in the pursuit.

In the early 1970s, Black, Scholes and Merton introduced the popular Black-Scholes-Merton (BSM) model [2,5]. Under the consideration, stock prices are assumed to follow geometric Brownian motion, while the volatility of the stock prices is fixed and no sudden jumps occur. However, classic BSM models often cannot fit ideally into market data observed nowadays [5]. This may be due to the fact that, in modern financial markets, not only stock prices are subject to risk, but also the estimate of the riskiness is typically subject to significant uncertainty. To incorporate additional sources of randomness into an option pricing model, Heston proposed a different approach by introducing the consideration of stochastic volatility [9].

There have been numerous recent publications on the numerical solution of Heston modeling equations. For instance, certain up-downwind first order algorithms are proposed and studied by

Preprints (www.preprints.org) | NOT PEER-REVIEWED | Posted: 29 October 2018 doi:10.20944/preprints201810.0649.v1

Peer-reviewed version available at Algorithms 2019, 12, 30; doi:10.3390/a12020030

Ma and Forsyth [15]. Stability analysis are also carried out via standard von Neumann analysis for Cauchy problems or problems with periodic boundary conditions [4,12]. Difficulties for more general stability analysis are primely due to the use of cross-derivative and boundary data [13]. Consequently, there has been no rigorous mathematical proof of the numerical stability for any second order scheme.

But cross-derivatives are essential to partial differential equations modeling a Heston Process. Further, Heston modeling formulations also require more realistic Dirichlet, Neumann, or mixed boundary conditions [1,9]. These have motivated our approaches. In this paper, we are particularly interested in computations based on a Heston put option model [4,5,8,10,12,22]. Similar investigations can also be carried out for a call option.

In particular, we consider the following two-dimensional Heston volatility model interpreting the behavior of the asset value S and its volatility y at time $t \geq 0$,

$$\begin{aligned} \frac{dS(t)}{S(t)} &= \mu dt + \sqrt{y(t)}dW_1(t), \\ dy(t) &= \kappa(\eta - y(t))dt + \sigma\sqrt{y(t)}dW_2(t), \\ \text{cov}(dW_1(t), dW_2(t)) &= \rho dt, \end{aligned}$$

where μ is the expected return of the asset, κ is the rate of reversion to the mean level of the volatility, η is the mean level of the volatility, $\sigma > 0$ is the volatility parameter, and $\text{cov}(u, v)$ is the covariance between u and v [9,21]. The two Wiener processes $W_1(t)$ and $W_2(t)$ describe the random noise in asset and volatility, respectively. They are assumed to be correlated with a constant correlation coefficient $\rho \in [-1, 1]$.

Let $v(S, y, t),\ t \geq 0$, denote the value of a European put option that is a function of asset price, volatility and time. An application of Itô's Lemma and the non-arbitrage principle with a construction of risk-less portfolio leads to [5,7,9,12,19],

$$v_t + \frac{1}{2}yS^2 v_{SS} + \rho\sigma y S v_{Sy} + \frac{\sigma^2 y}{2} v_{yy} + rSv_S + \kappa(\eta - y)v_y = rv,\ S, y > 0. \tag{1.1}$$

Let

$$v(S, y, T) = \max\{K - S, 0\},\quad S, y \geq 0,$$

be the terminal condition to use, where T is the payoff time and K is the strike price. We adopt the following mixed boundary conditions for $S, y > 0$ and $T > t \geq 0$ [4]:

$$\begin{aligned} v(0, y, t) &= Ke^{-r(T-t)}, \\ \lim_{S\to\infty} v(S, y, t) &= 0, \\ v_y(S, 0, t) &= 0, \\ \lim_{y\to\infty} v_y(S, y, t) &= 0. \end{aligned}$$

Preprints (www.preprints.org) | NOT PEER-REVIEWED | Posted: 29 October 2018 doi:10.20944/preprints201810.0649.v1

Peer-reviewed version available at Algorithms 2019, 12, 30; doi:10.3390/a12020030

Set $\tau = T - t$. Equation (1.1) can be rewritten as

$$v_\tau = \frac{yS^2}{2} v_{SS} + \rho\sigma y S v_{Sy} + \frac{\sigma^2 y}{2} v_{yy} + rSv_S + \kappa(\eta - y)v_y - rv, \quad T > \tau > 0.$$

Let $x = \ln \frac{S}{K}$, $u = \frac{v}{K} e^{r\tau}$. For $-\infty < x < \infty$, $y > 0$, $T > \tau > 0$ we observe that

$$u_\tau = \frac{y}{2} u_{xx} + \rho\sigma y u_{xy} + \frac{\sigma^2 y}{2} u_{yy} - \left(\frac{y}{2} - r\right) u_x + \kappa(\eta - y) u_y, \tag{1.2}$$

together with constraints [4,5,22],

$$\begin{aligned}
u(x,y,0) &= \max\{1 - e^x, 0\}, \quad -\infty < x < \infty,\ y > 0, && (1.3)\\
\lim_{x\to-\infty} u(x,y,\tau) &= 1, \quad y > 0,\ T \ge \tau > 0, && (1.4)\\
\lim_{x\to\infty} u(x,y,\tau) &= 0, \quad y > 0,\ T \ge \tau > 0, && (1.5)\\
u_y(x,0,\tau) &= 0, \quad -\infty < x < \infty,\ T \ge \tau > 0, && (1.6)\\
\lim_{y\to\infty} u_y(x,y,\tau) &= 0, \quad -\infty < x < \infty,\ T \ge \tau > 0. && (1.7)
\end{aligned}$$

We may extend the temporal domain for (1.2)-(1.7) by allowing $T = \infty$. Further, for the sake of computations, we consider a truncated spatial domain $\Omega = \{(x,y) : -X < x < X;\ 0 < y < Y\}$ for sufficiently large X and Y in the rest of our investigations.

In the next section, a nonuniform spacial mesh will be introduced. Based on it, a semi-discretized system will be derived for solving (1.2)-(1.7). Dynamically balanced up-downwind difference approximations will be presented. A general linear stability analysis will be implemented in Section 3. Computational experiments will be carried out in Section 4. Computationally evaluated rates of convergence of the scheme will also be provided. Finally, conclusions and future research intentions will be given in Section 5.

2. Results

2.1. Balanced up-downwind semi-discretized scheme

Let $-X = x_0 < x_1 < \cdots < x_M < x_{M+1} = X$, $0 = y_0 < y_1 < \cdots < y_N < y_{N+1} = Y$, for which $x_m - x_{m-1} = h_m$, $y_n - y_{n-1} = k_n$, $0 < h_m, k_n \ll 1$, $m = 1, 2, \ldots, M+1$, $n = 1, 2, \ldots, N+1$.

Let $z_{m,n} = z_{m,n}(\tau)$ be an approximation of $z(x_m, y_n, \tau)$, $0 \le m \le M+1$, $0 \le n \le N+1$, $0 < \tau < T$. Further, let $\Delta_{\ell,+}$, $\Delta_{\ell,-}$ and $\Delta_{\ell,0}$ be forward, backward and central difference operators

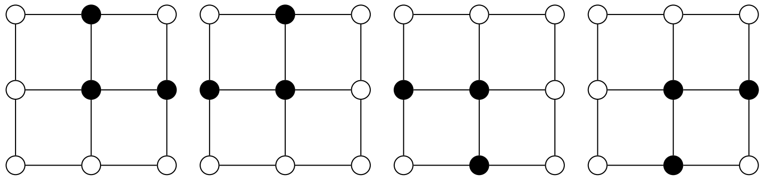

Figure 1. Computational stencil for (2.1) and (2.4) [frame 1]; (2.2) [frame 2]; (2.3) and (2.6) [frame 3]; (2.5) [frame 4]

in the ℓ-direction, respectively, where $\ell \in \{x, y\}$ [13,20]. Similarly, for appropriate indexes, we define

$$\begin{aligned}
\Delta^2_{x,0} z_{m,n} &= \frac{2z_{m+1,n}}{h_{m+1}(h_{m+1}+h_m)} - \frac{2z_{m,n}}{h_{m+1}h_m} + \frac{2z_{m-1,n}}{h_m(h_{m+1}+h_m)}, \\
\Delta^2_{y,0} z_{m,n} &= \frac{2z_{m,n+1}}{k_{n+1}(k_{n+1}+k_n)} - \frac{2z_{m,n}}{k_{n+1}k_n} + \frac{2z_{m,n-1}}{k_n(k_{n+1}+k_n)}.
\end{aligned}$$

We now approximate the diffusion terms in (1.2) by using the above, and derivatives in (1.6) and (1.7) via the following,

$$u_y(x_m, 0, \tau) \approx \frac{1}{h_y}\Delta_{y,+} u_{m,0}(\tau),\ u_y(x_m, Y, \tau) \approx \frac{1}{h_y}\Delta_{y,-} u_{m,N+1}(\tau),\ 0 < \tau < T.$$

We approximate the advection terms in (1.2) through three different channels depending upon relations between η and r.

Case 1: $\eta > 2r$.

$$\begin{aligned}
&u_x(x_m, y_n, \tau) \approx \Delta_{x,+} u_{m,n},\ u_y(x_m, y_n, \tau) \approx \Delta_{y,+} u_{m,n}, && 2r \ge y > 0, && (2.1)\\
&u_x(x_m, y_n, \tau) \approx \Delta_{x,-} u_{m,n},\ u_y(x_m, y_n, \tau) \approx \Delta_{y,+} u_{m,n}, && \eta \ge y > r, && (2.2)\\
&u_x(x_m, y_n, \tau) \approx \Delta_{x,-} u_{m,n},\ u_y(x_m, y_n, \tau) \approx \Delta_{y,-} u_{m,n}, && Y > y > \eta. && (2.3)
\end{aligned}$$

Case 2: $\eta \le 2r$.

$$\begin{aligned}
&u_x(x_m, y_n, \tau) \approx \Delta_{x,+} u_{m,n},\ u_y(x_m, y_n, \tau) \approx \Delta_{y,+} u_{m,n}, && \eta \ge y > 0, && (2.4)\\
&u_x(x_m, y_n, \tau) \approx \Delta_{x,+} u_{m,n},\ u_y(x_m, y_n, \tau) \approx \Delta_{y,-} u_{m,n}, && 2r \ge y > \eta, && (2.5)\\
&u_x(x_m, y_n, \tau) \approx \Delta_{x,-} u_{m,n},\ u_y(x_m, y_n, \tau) \approx \Delta_{y,-} u_{m,n}, && Y > y > 2r. && (2.6)
\end{aligned}$$

Define

$$h_{\min} = \min_{m=1,2\cdots M} h_m,\ h_{\max} = \max_{m=1,2\cdots M} h_m;\ k_{\min} = \min_{n=1,2\cdots N} k_n,\ k_{\max} = \max_{n=1,2\cdots N} k_n.$$

We now approximate the cross-derivative in (1.2) dynamically. To this end, we have

Preprints (www.preprints.org) | NOT PEER-REVIEWED | Posted: 29 October 2018 doi:10.20944/preprints201810.0649.v1

Peer-reviewed version available at Algorithms 2019, 12, 30; doi:10.3390/a12020030

70 2.1.1. Case for $\rho \in [-1, 0]$.

For the smoothness of nonuniform grids [20], we require that

$$-\rho k_{\max} \le \sigma h_{\min} \le \sigma h_{\max} \le -\frac{1}{\rho} k_{\min}. \tag{2.7}$$

We propose that

$$u_{xy}(x_m, y_n, \tau) = \frac{1}{2}(\Delta_{x,+}\Delta_{y,-} + \Delta_{x,-}\Delta_{y,+})u_{m,n}(\tau) + \mathcal{O}(h_{\max} + k_{\max}). \tag{2.8}$$

Substitute all spacial derivative approximations into (1.2) and let w denote the approximate solution to u. We acquire the following linear system,

$$w'(\tau) = Aw(\tau) + f(\tau), \tag{2.9}$$

71 where $w, f \in \mathbb{R}^{MN}$ and $A \in \mathbb{R}^{MN \times MN}$ is block tridiagonal in the form of

$$A = \begin{bmatrix} D_1 & Q_1 & \cdots & \cdots & \cdots & 0 \\ P_2 & D_2 & Q_2 & \cdots & \cdots & 0 \\ \vdots & \ddots & \ddots & \ddots & \cdots & \vdots \\ \vdots & \cdots & P_{M-2} & D_{M-2} & Q_{M-2} & 0 \\ \cdots & \cdots & \cdots & P_{M-1} & D_{M-1} & Q_{M-1} \\ 0 & \cdots & \cdots & \cdots & P_M & D_M \end{bmatrix},$$

Preprints (www.preprints.org) | NOT PEER-REVIEWED | Posted: 29 October 2018 doi:10.20944/preprints201810.0649.v1

Peer-reviewed version available at Algorithms 2019, 12, 30; doi:10.3390/a12020030

where $P_i, D_j, Q_k \in \mathbb{R}^{N\times N}$, $i = 2,3,\ldots,M$; $j = 1,2,\ldots,M$; $k = 1,2,\ldots,M-1$. Nontrivial entries of the matrices P_m, D_m and Q_m for their respective ranges of m are as follows.

$$
\begin{aligned}
p_{n,n}^{(m)} &= \begin{cases} \dfrac{y_n}{h_m(h_m+h_{m+1})} + \dfrac{\rho\sigma y_n}{2h_m k_{n+1}}, & 0 < y_n \le 2r, \\ \dfrac{y_n}{h_m(h_m+h_{m+1})} + \dfrac{\rho\sigma y_n}{2h_m k_{n+1}} + \dfrac{y_n - 2r}{2h_m}, & 2r < y_n < Y - k_{N+1}, \\ \dfrac{y_N}{h_m(h_m+h_{m+1})} + \dfrac{y_N - 2r}{2h_m}, & y_n = Y - k_{N+1}; \end{cases} \\
p_{n,n+1}^{(m)} &= -\frac{\rho\sigma y_n}{2h_m k_n}; \\
d_{n,n-1}^{(m)} &= \begin{cases} \dfrac{\sigma^2 y_n}{k_n(k_n+k_{n+1})} + \dfrac{\rho\sigma y_n}{2h_{m+1}k_n}, & k_1 < y_n \le \eta, \\ \dfrac{\sigma^2 y_n}{k_n(k_n+k_{n+1})} + \dfrac{\rho\sigma y_n}{2h_{m+1}k_n} - \dfrac{\kappa(\eta - y_n)}{k_n}, & \eta < y_n \le Y - k_{N+1}; \end{cases} \\
d_{n,n}^{(m)} &= \begin{cases} \alpha_{m,1} + \dfrac{y_1 - 2r}{2h_{m+1}} - \dfrac{\kappa(\eta - y_1)}{k_2}, & y_n = k_1, \\ \beta_{m,n} + \dfrac{y_n - 2r}{2h_{m+1}} - \dfrac{\kappa(\eta - y_n)}{k_{n+1}}, & k_1 < y_n \le 2r, \\ \beta_{m,n} - \dfrac{y_n - 2r}{2h_m} - \dfrac{\kappa(\eta - y_n)}{k_{n+1}}, & 2r < y_n \le \eta, \\ \beta_{m,n} - \dfrac{y_n - 2r}{2h_m} + \dfrac{\kappa(\eta - y_n)}{k_n}, & \eta < y_n < Y - k_{N+1}, \\ \gamma_{m,N} - \dfrac{y_N - 2r}{2h_m} + \dfrac{\kappa(\eta - y_N)}{k_N}, & y_N = Y - k_{N+1}; \end{cases} \\
d_{n,n+1}^{(m)} &= \begin{cases} \dfrac{\sigma^2 y_n}{k_{n+1}(k_n+k_{n+1})} + \dfrac{\rho\sigma y_n}{2h_m k_{n+1}} + \dfrac{\kappa(\eta - y_n)}{k_{n+1}}, & 0 < y_n \le \eta, \\ \dfrac{\sigma^2 y_n}{k_{n+1}(k_n+k_{n+1})} + \dfrac{\rho\sigma y_n}{2h_m k_{n+1}}, & \eta < y_n < Y - k_{N+1}; \end{cases} \\
q_{n,n-1}^{(m)} &= -\frac{\rho\sigma y_n}{2h_{m+1}k_n}, \quad y_n > k_1; \\
q_{n,n}^{(m)} &= \begin{cases} \dfrac{y_1}{h_{m+1}(h_m+h_{m+1})} - \dfrac{y_1 - 2r}{2h_{m+1}}, & y_n = k_1, \\ \dfrac{y_n}{h_{m+1}(h_m+h_{m+1})} + \dfrac{\rho\sigma y_n}{2h_{m+1}k_n} - \dfrac{y_n - 2r}{2h_{m+1}}, & k_1 < y \le 2r, \\ \dfrac{y_n}{h_{m+1}(h_m+h_{m+1})} + \dfrac{\rho\sigma y_n}{2h_{m+1}k_n}, & 2r < y_n \le Y - k_{N+1}, \end{cases}
\end{aligned}
$$

where

$$\begin{aligned}
\alpha_{m,n} &= -\frac{y_n}{h_m h_{m+1}} - \frac{\sigma^2 y_n}{k_{n+1}(k_n + k_{n+1})} - \frac{\rho\sigma y_n}{2h_m k_{n+1}}, \\
\beta_{m,n} &= -\frac{y_n}{h_m h_{m+1}} - \frac{\sigma^2 y_n}{k_n k_{n+1}} - \frac{\rho\sigma y_n}{2h_{m+1} k_n} - \frac{\rho\sigma y_n}{2h_m k_{n+1}}, \\
\gamma_{m,n} &= -\frac{y_n}{h_m h_{m+1}} - \frac{\sigma^2 y_n}{k_n(k_n + k_{n+1})} - \frac{\rho\sigma y_n}{2h_{m+1} k_n}.
\end{aligned}$$

It is observed that in the event if $\rho = -1$, we have the following due to (2.7):

$$h_{\min} = h_{\max} = h,\ k_{\min} = k_{\max} = k,\ k = \sigma h,$$

which indicate that uniform spacial grids must be employed. Thus, (2.9) reduces to

$$w'(\tau) = A_s w(\tau) + f_s(\tau).$$

Nontrivial entries of A_s are readily to obtain based on above discussions.

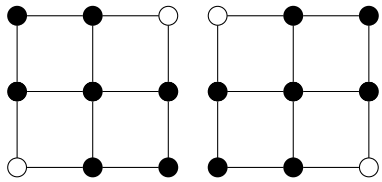

Figure 2. Computational stencil of (2.8) [left] and (2.11) [right].

2.1.2. Case for $\rho \in (0, 1]$.

We need the following restrictions on mesh steps in the case [20]:

$$\rho k_{\max} \leq \sigma h_{\min} \leq \sigma h_{\max} \leq \frac{1}{\rho} k_{\min}. \tag{2.10}$$

Apparently, when $\rho = 1$, the above implies that a uniform spacial mesh with $h = \sigma k$ must be used.

Different from (2.8), we consider a new dynamically balanced cross-derivative approximation,

$$u_{xy}(x_m, y_n, \tau) = \frac{1}{2}(\Delta_{x,-}\Delta_{y,-} + \Delta_{x,+}\Delta_{y,+})u_{m,n}(\tau) + \mathcal{O}(h_{\max} + k_{\max}). \tag{2.11}$$

Computational stencils for (2.8) and (2.11) are shown in Figure 2.

Peer-reviewed version available at Algorithms 2019, 12, 30; doi:10.3390/a12020030

In this circumstance, we obtain the following new system,

$$w'(\tau) = \tilde{A}w(\tau) + \tilde{f}(\tau), \tag{2.12}$$

80 where $w, \tilde{f}(\tau) \in \mathbb{R}^{MN}$ and $\tilde{A} \in \mathbb{R}^{MN\times MN}$ is block tridiagonal, that is,

$$\tilde{A} \;=\; \begin{bmatrix} \tilde{D}_1 & \tilde{Q}_1 & \cdots & \cdots & \cdots & 0 \\ \tilde{P}_2 & \tilde{D}_2 & \tilde{Q}_2 & \cdots & \cdots & 0 \\ \vdots & \ddots & \ddots & \ddots & \cdots & \vdots \\ \vdots & \cdots & \tilde{P}_{M-2} & \tilde{D}_{M-2} & \tilde{Q}_{M-2} & 0 \\ \cdots & \cdots & \cdots & \tilde{P}_{M-1} & \tilde{D}_{M-1} & \tilde{Q}_{M-1} \\ 0 & \cdots & \cdots & \cdots & \tilde{P}_M & \tilde{D}_M \end{bmatrix}.$$

81 Nontrivial entries of $\tilde{P}_m$, $\tilde{D}_m$ and $\tilde{Q}_m$ within their respective ranges of m are given by

$$\tilde{p}^{(m)}_{n,n-1} \;=\; \frac{\rho\sigma y_n}{2h_m k_n}, \quad y_n > k_1;$$

$$\tilde{p}^{(m)}_{n,n} \;=\; \begin{cases} \dfrac{y_1}{h_m(h_m+h_{m+1})}, & y_n = k_1, \\ \dfrac{y_n}{h_m(h_m+h_{m+1})} - \dfrac{\rho\sigma y_n}{2h_m k_n}, & k_1 < y_n \le 2r, \\ \dfrac{y_n}{h_m(h_m+h_{m+1})} - \dfrac{\rho\sigma y_n}{2h_m k_n} + \dfrac{y_n - 2r}{2h_m}, & 2r < y_n \le Y - k_{N+1}; \end{cases}$$

$$\tilde{r}^{(m)}_{n,n-1} \;=\; \begin{cases} \dfrac{\sigma^2 y_n}{k_n(k_n+k_{n+1})} - \dfrac{\rho\sigma y_n}{2h_m k_n}, & k_1 < y_n \le \eta, \\ \dfrac{\sigma^2 y_n}{k_n(k_n+k_{n+1})} - \dfrac{\rho\sigma y_n}{2h_m k_n} - \dfrac{\kappa(\eta - y_n)}{k_n}, & \eta < y_n \le Y - k_{N+1}; \end{cases}$$

$$\tilde{r}^{(m)}_{n,n} \;=\; \begin{cases} \tilde{\alpha}_{m,1} + \dfrac{y_1 - 2r}{2h_{m+1}} - \dfrac{\kappa(\eta - y_1)}{k_{n+1}}, & y_1 = k_1, \\ \tilde{\beta}_{m,n} + \dfrac{y_n - 2r}{2h_{m+1}} - \dfrac{\kappa(\eta - y_n)}{k_{n+1}}, & k_1 < y_n \le 2r, \\ \tilde{\beta}_{m,n} - \dfrac{y_n - 2r}{2h_m} - \dfrac{\kappa(\eta - y_n)}{k_{n+1}}, & 2r < y_n \le \eta, \\ \tilde{\beta}_{m,n} - \dfrac{y_n - 2r}{2h_m} + \dfrac{\kappa(\eta - y_n)}{k_n}, & \eta < y_n < Y - k_{N+1}, \\ \tilde{\gamma}_{m,N} - \dfrac{y_N - 2r}{2h_m} + \dfrac{\kappa(\eta - y_N)}{k_N}, & y_N = Y - k_{N+1}; \end{cases}$$

Peer-reviewed version available at Algorithms 2019, 12, 30; doi:10.3390/a12020030

$$\begin{aligned}
\tilde{r}^{(m)}_{n,n+1} &= \begin{cases} \dfrac{\sigma^2 y_n}{k_{n+1}(k_n+k_{n+1})} - \dfrac{\rho\sigma y_n}{2h_{m+1}k_{n+1}} + \dfrac{\kappa(\eta - y_n)}{k_{n+1}}, & 0 < y_n \le \eta, \\ \dfrac{\sigma^2 y_n}{k_{n+1}(k_n+k_{n+1})} - \dfrac{\rho\sigma y_n}{2h_{m+1}k_{n+1}}, & \eta < y_n < Y - k_{N+1}; \end{cases} \\
\tilde{q}^{(m)}_{n,n} &= \begin{cases} \dfrac{y_n}{h_{m+1}(h_m+h_{m+1})} - \dfrac{\rho\sigma y_n}{2h_{m+1}k_{n+1}} - \dfrac{y_n - 2r}{2h_{m+1}}, & 0 < y_n \le 2r, \\ \dfrac{y_n}{h_{m+1}(h_m+h_{m+1})} - \dfrac{\rho\sigma y_n}{2h_{m+1}k_{n+1}}, & 2r < y_n < Y - k_{N+1}, \\ \dfrac{y_N}{h_{m+1}(h_m+h_{m+1})}, & y_N = Y - k_{N+1}; \end{cases} \\
\tilde{q}^{(m)}_{n,n+1} &= \frac{\rho\sigma y_n}{2h_{m+1}k_{n+1}}, \quad 0 < y_n < Y - k_{N+1},
\end{aligned}$$

82 where

$$\begin{aligned}
\tilde{\alpha}_{m,n} &= -\frac{y_n}{h_m h_{m+1}} - \frac{\sigma^2 y_n}{k_{n+1}(k_n+k_{n+1})} + \frac{\rho\sigma y_n}{2h_{m+1}k_{n+1}} + \frac{\rho\sigma y_n}{2h_m k_n}, \\
\tilde{\beta}_{m,n} &= -\frac{y_n}{h_m h_{m+1}} - \frac{\sigma^2 y_n}{k_n k_{n+1}} + \frac{\rho\sigma y_n}{2h_{m+1}k_{n+1}} + \frac{\rho\sigma y_n}{2h_m k_n}, \\
\tilde{\gamma}_{m,n} &= -\frac{y_n}{h_m h_{m+1}} - \frac{\sigma^2 y_n}{k_n(k_n+k_{n+1})} + \frac{\rho\sigma y_n}{2h_m k_n}.
\end{aligned}$$

The semi-discretized method (2.12) reduces to a uniform scheme when $\rho = 1$, that is,

$$w'(\tau) = \frac{1}{2h^2}\tilde{A}_s w(\tau) + \tilde{f}(\tau).$$

83 Nontrivial elements of $\tilde{A}$ can be determined from simplifications of the above formulae.

84 *2.2. Numerical stability*

It is readily to verify that the the solution to (2.9) is

$$w(\tau_{n+1}) = e^{\Delta\tau A}w(\tau_n) + \int_{\tau_n}^{\tau_{n+1}} e^{(t-\tau_n)A} f(t)dt, \quad n = 0, 1, \ldots, \tag{2.1}$$

85 where $\tau_n = n\Delta\tau$. The formal solution to (2.12) is similar. We have

Lemma 1. [13,18] *The semi-discretized schemes* (2.9) *and* (2.12) *are stable if*

$$\lim_{h_{max}, k_{max}\to 0}\left(\max_{\tau\in[0,\tau^*]}\left\|e^{\tau A}\right\|_2\right) \le c(\tau^*), \quad \lim_{h_{max}, k_{max}\to 0}\left(\max_{\tau\in[0,\tau^*]}\left\|e^{\tau \tilde{A}}\right\|_2\right) \le c(\tau^*),$$

86 *where* $\tau^* \in (0, T)$.

Peer-reviewed version available at Algorithms 2019, 12, 30; doi:10.3390/a12020030

Lemma 2. [13] *Let $B \in \mathbb{C}^{d\times d}$. Then $\sigma(B) \subset \cup_{i=1}^{d} S_i$, where*

$$S_i = \left\{ z \in C : |z - b_{i,i}| \le \sum_{j=1, j\ne i}^{d} |b_{i,j}| \right\}$$

are Geršhgorin discs and $\sigma(B)$ is the set containing all eigenvalues of B. Moreover, $\lambda \in \sigma(B)$ may lie on ∂S_{i^0} for some $i^0 \in \{1, 2, \dots, d\}$ only if $\lambda \in \partial S_i$ for all $i = 1, 2, \dots, d$.

Lemma 3. [17] *The matrix exponential, e^{tA}, tends to a zero matrix as $t \to +\infty$ if and only if all the eigenvalues of A have strictly negative real parts.*

Theorem 4. *The semi-discretized schemes (2.9) and (2.12) are linearly stable.*

Proof. We will only need to show the case of $\rho \in (0, 1]$, $\eta > 2r$ for (2.9), since extensions of our results for other cases are technically imminent. Thus, we only need to show that each of the MN Geršhgorin discs of A lies on the left side of the complex plane. In fact, there are five types of the Geršhgorin discs to consider:

1. discs centered at an internal mesh point;
2. discs centered on one of the Dirichlet boundaries;
3. discs centered on the Neumann boundary;
4. discs centered at one of the intersection mesh points of two Dirichlet boundaries;
5. discs centered at one of the intersection mesh points of one Dirichlet boundary and the Neumann boundary.

We provide detailed proofs for the first three types of discs. Similar arguments can be applied to the rest cases.

CASE 1: In this situation, we first consider the situation in which $\eta < y_n \le Y$. Let $z \in S_i$ be any complex number, where S_i is a Geršhgorin disc centered at an internal point of the spacial grids. Thus,

$$\begin{aligned}
&\left| z + \frac{y_n}{h_m h_{m+1}} + \frac{\sigma^2 y_n}{k_n k_{n+1}} - \frac{\rho\sigma y_n}{2h_{m+1}k_{n+1}} - \frac{\rho\sigma y_n}{2h_m k_n} + \frac{y_n - 2r}{2h_m} - \frac{\kappa(\eta - y_n)}{k_n} \right| \\
&\quad \le \left| \frac{\sigma^2 y_n}{k_n(k_n + k_{n+1})} - \frac{\rho\sigma y_n}{2h_m k_n} - \frac{\kappa(\eta - y_n)}{k_n} \right| + \left| \frac{\sigma^2 y_n}{k_{n+1}(k_n + k_{n+1})} - \frac{\rho\sigma y_n}{2h_{m+1}k_{n+1}} \right| \\
&\quad + \left| \frac{y_n}{h_{m+1}(h_m + h_{m+1})} - \frac{\rho\sigma y_n}{2h_{m+1}k_{n+1}} \right| + \left| \frac{\rho\sigma y_n}{2h_{m+1}k_{n+1}} \right| + \left| \frac{\rho\sigma y_n}{2h_m k_n} \right| \\
&\quad + \left| \frac{y_n}{h_m(h_m + h_{m+1})} - \frac{\rho\sigma y_n}{2h_m k_n} + \frac{y_n - 2r}{2h_m} \right|.
\end{aligned} \tag{2.2}$$

Let α be the real part of z. Since we are concerned only about the upper bound of the real part of the eigenvalues, we may replace z by α via a triangle inequality, and remove absolute value sign on the left hand side of (2.2). As a consequence, (2.2) renders to

$$\begin{aligned}
\alpha + \frac{y_n}{h_m h_{m+1}} + \frac{\sigma^2 y_n}{k_n k_{n+1}} - \frac{\rho\sigma y_n}{2h_{m+1}k_{n+1}} - \frac{\rho\sigma y_n}{2h_m k_n} + \frac{y_n - 2r}{2h_m} - \frac{\kappa(\eta - y_n)}{k_n} \\
\leq \left| \frac{\sigma^2 y_n}{k_n(k_n + k_{n+1})} - \frac{\rho\sigma y_n}{2h_m k_n} - \frac{\kappa(\eta - y_n)}{k_n} \right| + \left| \frac{\sigma^2 y_n}{k_{n+1}(k_n + k_{n+1})} - \frac{\rho\sigma y_n}{2h_{m+1}k_{n+1}} \right| \\
+ \left| \frac{y_n}{h_{m+1}(h_m + h_{m+1})} - \frac{\rho\sigma y_n}{2h_{m+1}k_{n+1}} \right| + \left| \frac{\rho\sigma y_n}{2h_{m+1}k_{n+1}} \right| + \left| \frac{\rho\sigma y_n}{2h_m k_n} \right| \\
+ \left| \frac{y_n}{h_m(h_m + h_{m+1})} - \frac{\rho\sigma y_n}{2h_m k_n} + \frac{y_n - 2r}{2h_m} \right|. \qquad (2.3)
\end{aligned}$$

Recall (2.10) and that $\rho > 0$. We have

$$\frac{2}{\rho\sigma}k_n,\ \frac{2}{\rho\sigma}k_{n+1} \geq h_m + h_{m+1} \text{ and } h_m,\ h_{m+1} \geq \frac{\rho}{\sigma}(k_n + k_{n+1}).$$

The above indicates that

$$\begin{aligned}
\frac{\sigma^2 y_n}{k_n(k_n + k_{n+1})} &\geq \frac{\rho\sigma y_n}{2h_m k_n}, \\
\frac{\sigma^2 y_n}{k_{n+1}(k_n + k_{n+1})} &\geq \frac{\rho\sigma y_n}{2h_{m+1}k_{n+1}}, \\
\frac{y_n}{h_{m+1}(h_m + h_{m+1})} &\geq \frac{\rho\sigma y_n}{2h_{m+1}k_{n+1}}, \\
\frac{y_n}{h_m(h_m + h_{m+1})} &\geq \frac{\rho\sigma y_n}{2h_m k_n}.
\end{aligned}$$

Furthermore, since $y > \eta > 2r$, we conclude that

$$-\frac{\kappa(\eta - y_n)}{k_n} \geq 0 \text{ and } \frac{y_n - 2r}{2h_m} \geq 0.$$

Therefore, the term inside each pair of absolute signs in (2.3) must be positive. We may remove all absolute signs in (2.3), and, subsequently, yields

$$\alpha \leq 0,$$

which is what we expect. Generalizations of the discussion for cases involving $y \leq \eta$ are straightforward. Therefore all eigenvalues contained in S_i must lie on the left half of the complex plane.

Preprints (www.preprints.org) | NOT PEER-REVIEWED | Posted: 29 October 2018 doi:10.20944/preprints201810.0649.v1

Peer-reviewed version available at *Algorithms* **2019**, *12*, 30; doi:10.3390/a12020030

CASE 2: Without loss of the generality, we consider the case of $x = x_1$ and $\eta < y < Y$. Thus, for any complex number $z \in S_i$, where S_i is a Geršhgorin disc satisfying

$$\begin{aligned}&\left|z + \frac{y_n}{h_m h_{m+1}} + \frac{\sigma^2 y_n}{k_n k_{n+1}} - \frac{\rho\sigma y_n}{2h_{m+1}k_{n+1}} - \frac{\rho\sigma y_n}{2h_m k_n} + \frac{y_n - 2r}{2h_m} - \frac{\kappa(\eta - y_n)}{k_n}\right| \\ &\leq \left|\frac{\sigma^2 y_n}{k_n(k_n + k_{n+1})} - \frac{\rho\sigma y_n}{2h_m k_n} - \frac{\kappa(\eta - y_n)}{k_n}\right| + \left|\frac{\sigma^2 y_n}{k_{n+1}(k_n + k_{n+1})} - \frac{\rho\sigma y_n}{2h_{m+1}k_{n+1}}\right| \\ &+ \left|\frac{y_n}{h_{m+1}(h_m + h_{m+1})} - \frac{\rho\sigma y_n}{2h_{m+1}k_{n+1}}\right| + \left|\frac{\rho\sigma y_n}{2h_{m+1}k_{n+1}}\right|.\end{aligned}$$

Similar to the previous case, we take α, the real part of z. Thus,

$$\alpha \leq \frac{y_n}{h_{m+1}}\left(\frac{1}{h_m + h_{m+1}} - \frac{1}{h_m}\right) - \frac{y_n - 2r}{2h_m} < 0.$$

The above apparently implies that such an S_i must lie strictly on the left half of the complex plane, and the origin cannot be on its boundary. This ensures our expectation.

CASE 3: In the circumstance, Geršhgorin discs, S_i, concerned are centered at boundary points where a Neumann condition is imposed. Hence, for any $z \in S_i$ we have

$$\begin{aligned}&\left|z + \frac{y_N}{h_m h_{m+1}} + \frac{\sigma^2 y_N}{k_N(k_{N+1} + k_N)} - \frac{\rho\sigma y_N}{2h_m k_N} + \frac{y_N - 2r}{2h_m} - \frac{\kappa(\eta - y_N)}{k_N}\right| \\ &\leq \left|\frac{\sigma^2 y_N}{k_N(k_N + k_{N+1})} - \frac{\rho\sigma y_N}{2h_m k_N} - \frac{\kappa(\eta - y_N)}{k_N}\right| + \left|\frac{y_N}{h_{m+1}(h_m + h_{m+1})}\right| \\ &+ \left|\frac{\rho\sigma y_N}{2h_m k_N}\right| + \left|\frac{y_N}{h_m(h_m + h_{m+1})} - \frac{\rho\sigma y_N}{2h_m k_N} + \frac{y_N - 2r}{2h_m}\right|.\end{aligned}$$

The above indicates that α, the real part of z, must satisfy

$$\alpha \leq \frac{y_N}{(h_m + h_{m+1})^2} - \frac{y_N}{h_m h_{m+1}} < 0.$$

Recall Lemma 3.2. Since the origin cannot lie on the boundary of every Geršhgorin disc, combining results from the three cases, we conclude immediately that all eigenvalues of A must be strictly on the left half complex plane. Thus, we must have

$$\lim_{h_{max}, k_{max} \to 0}\left(\max_{\tau \in [0, \tau^*]}\left\|e^{\tau A}\right\|_2\right) \leq c(\tau^*).$$

The above completes our proof. □

2.3. *Computational experiments*

Consider (1.2)-(1.7). Similar to discussions in [22], we fix $X = 8$, $Y = 1$. We first concentrate on experiments with $\rho = -0.5$ and $T = 0.5$. Next, to test against extreme cases in the option

Preprints (www.preprints.org) | NOT PEER-REVIEWED | Posted: 29 October 2018 doi:10.20944/preprints201810.0649.v1

Peer-reviewed version available at Algorithms 2019, 12, 30; doi:10.3390/a12020030

Table 1. Key parameter values for numerical simulations

.

key parameter	value used
strike price	$K = 100$
interest rate	$r = 0.05$
mean reversion speed	$\kappa = 2$
long-run mean of volatility	$\eta = 0.1$

market, we proceed with $\rho = -1$ and $T = 5$. For demonstrating the numerical solution and its rate of convergence estimates, we first consider uniform spacial grids. To this end, we may denote that

$$h_m = h,\ k_n = k = \sigma h,\ \ m = 1, 2, \ldots, M;\ n = 1, 2, \ldots, N.$$

Results over nonuniform grids will be presented later on.

Some key parameters used are shown in Table 1. Further, a Crank-Nicolson type temporal integrator will be utilized for advancing our semi-discretized system (2.9), (2.12), with $\Delta\tau$ as the temporal step [18]. It has been known that $\lambda = \Delta\tau/c^2$, where $c = \min\{h, k\}$, play an effective role of the Courant number [14,16]. We experiment with different values of λ varying from 0.5 to 1.

Our semi-discretized scheme is expected to be up to the first order in convergence in space. To numerically examine this through experiments, we employ a generalized Milne's device [13,20]. Then, for a selected terminal time T, we denote the numerical solution at point (x_m, y_n, T), $1 \le m \le M; 1 \le n \le N$, as $u_{m,n;h}$ for any particular spatial step $0 < h \ll 1$. Likewise, we let $u_{m,n;h/2}$ and $u_{m,n;h/4}$ be computed solutions obtained by using $h/2$ and $h/4$, respectively. Thus, the point-wise rate of spatial convergence at T can be evaluated via

$$R^h_{m,n} \approx \frac{1}{\ln 2} \ln \frac{|u_{m,n;h} - u_{m,n;h/2}|}{|u_{m,n;h/2} - u_{m,n;h/4}|}.$$

Most of our experiments are accomplished on Apple workstations. Matlab platforms without parallelizations are used throught operations.

Let $h = 0.01$ and $\sigma = 1$. For simplicity of notations, we use the same letter v for the approximate solution to (1.1). We show the solution v for $\rho = -0.5$ and $\rho = -1$ in Figure 3 and Figure 5 , respectively. To see more precisely solution profiles, we show corresponding contour maps next to the surfaces. It can be observed that the European put option price is a decreasing function of the stock price S. This coincides well with the financial theory that a put option price should have a negative correlation with the underline stock price [1,11]. To examine further the delicate relationship between a put option price and its volatility, we plot an average numerical solution $\bar{v}(y, t)$ taken across different stock prices with respect to the volatility in Figure 7. The simulated computational result is exactly what we would expect, since a put option price should be positively correlated with the volatility [11,16].

Preprints (www.preprints.org) | NOT PEER-REVIEWED | Posted: 29 October 2018 doi:10.20944/preprints201810.0649.v1

Peer-reviewed version available at *Algorithms* **2019**, *12*, 30; doi:10.3390/a12020030

Table 2. Rates of convergence R^h_{PW} observed with $\sigma = 1$, $\rho = -0.5$ and $T = 0.5$.

mesh steps	rconv. rates	$\lambda = 0.5$	$\lambda = 0.75$	$\lambda = 1$
$h = 0.01$	$\min_{m,n}(R^h_{m,n})$	0.6193	0.6134	0.6026
	$\max_{m,n}(R^h_{m,n})$	1.0024	0.9976	0.9811
	$\text{mean}_{m,n}(R^h_{m,n})$	0.9026	0.90438	0.9053
$h = 0.02$	$\min_{m,n}(R^h_{m,n})$	0.6324	0.6221	0.6206
	$\max_{m,n}(R^h_{m,n})$	0.9674	1.0007	1.0151
	$\text{mean}_{m,n}(R^h_{m,n})$	0.8342	0.8300	0.8296
$h = 0.03$	$\min_{m,n}(R^h_{m,n})$	0.5824	0.5971	0.6179
	$\max_{m,n}(R^h_{m,n})$	0.9941	0.9437	0.9586
	$\text{mean}_{m,n}(R^h_{m,n})$	0.7952	0.8015	0.8142

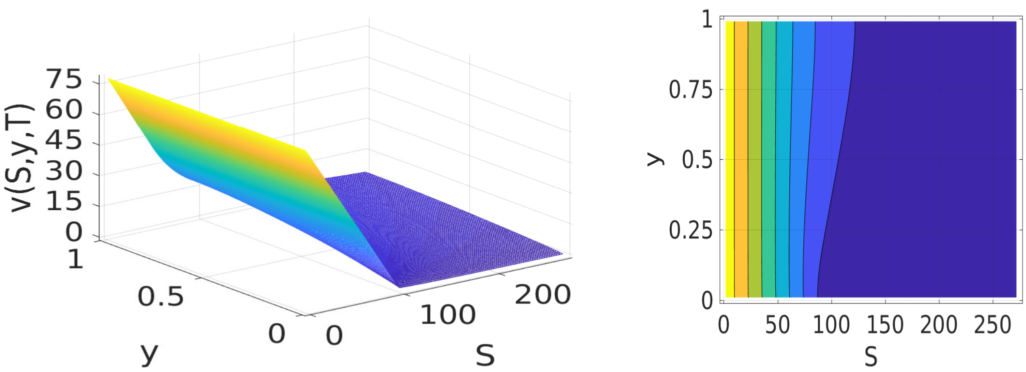

Figure 3. LEFT: Price of an European put option at $T = 0.5$ and for $\rho = -0.5$; RIGHT: Corresponding contour map

146 To exam actual performances of our dynamically balanced algorithms, we plot computed rate of convergence surfaces for cases when $\rho = -0.5$ and $\rho = -1$ in Figure 4 and Figure 6, respectively. In addition, a summary of point-wise convergence rates for the circumstance as $\rho = -0.5$, $T = 0.5$ on different spacial grids is given in Table 2. Minor disturbances can be observed in regions where the solution changes fast, in particularly in extreme situations with $\rho = -1$ as being demonstrated in Figure 6.

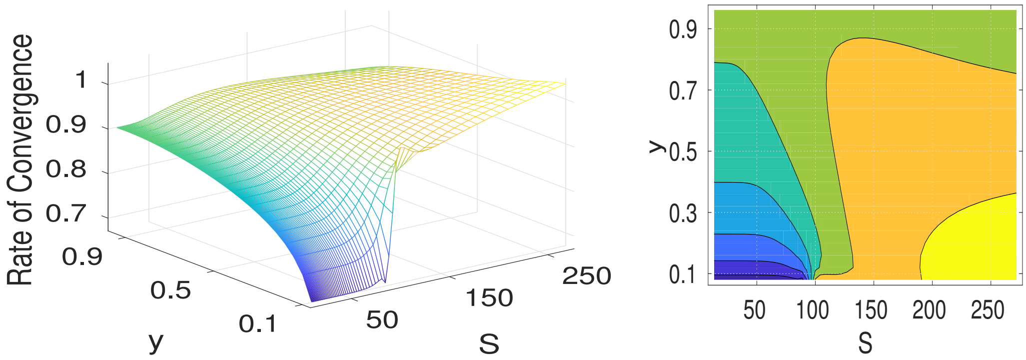

Figure 4. LEFT: Point-wise rate of convergence estimate at $T = 0.5$ and for $\rho = -0.5$; RIGHT: Corresponding contour map

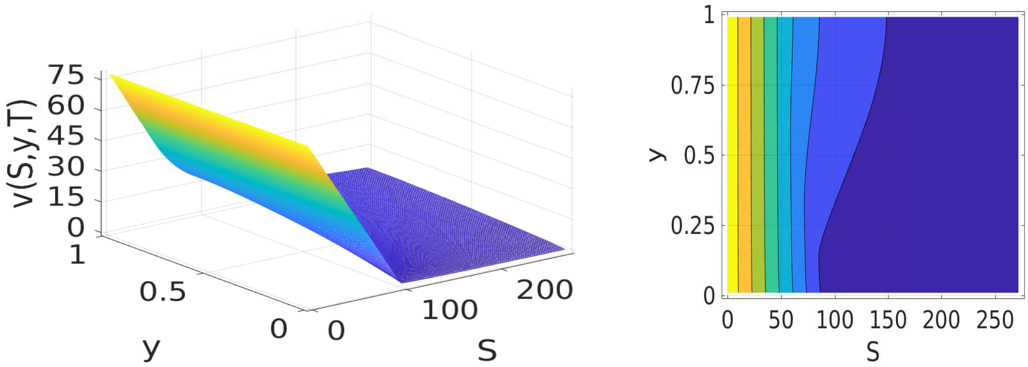

Figure 5. LEFT: Price of an European put option at $T = 5$ and for $\rho = -1$; RIGHT: Corresponding contour map

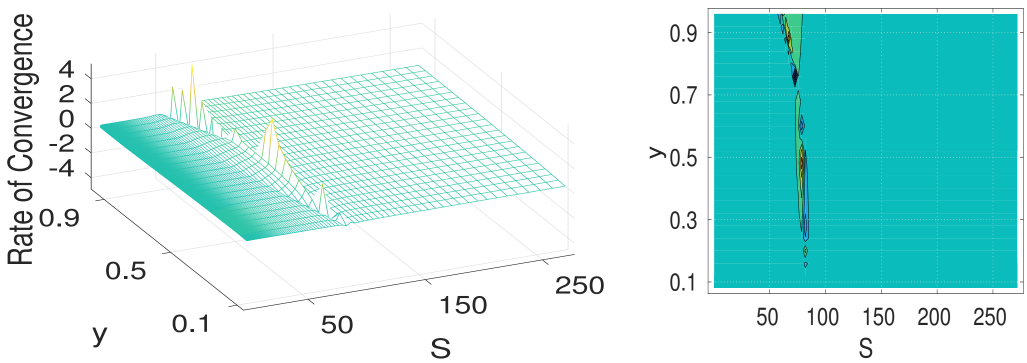

Figure 6. LEFT: Point-wise rate of convergence estimate at $T = 5$ and for $\rho = -1$. RIGHT: Corresponding contour map

Preprints (www.preprints.org) | NOT PEER-REVIEWED | Posted: 29 October 2018 doi:10.20944/preprints201810.0649.v1

Peer-reviewed version available at *Algorithms* **2019**, *12*, 30; doi:10.3390/a12020030

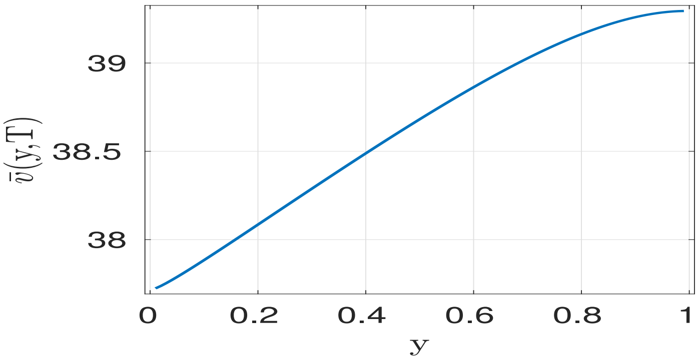

Figure 7. Relation between average price of an European put option with volatility at $T = 0.5$ and for $\rho = -0.5$.

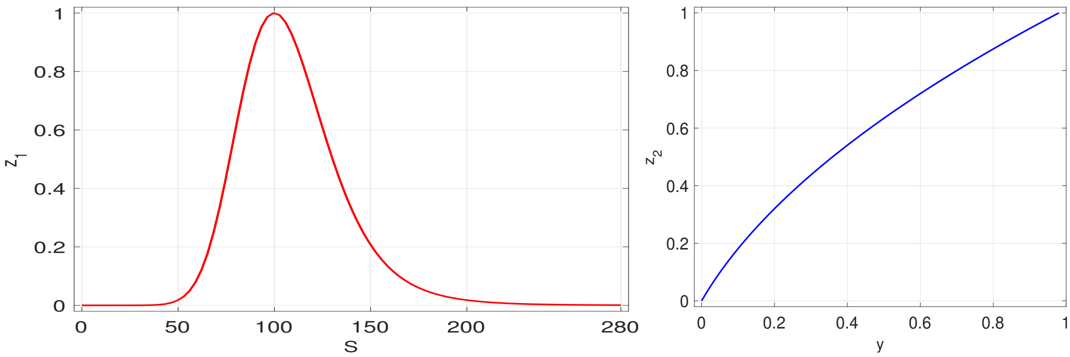

Figure 8. LEFT: Nonlinear mesh distribution governing function z_1 in the S-direction; RIGHT: Nonlinear mesh distribution governing function z_2 in the y-direction

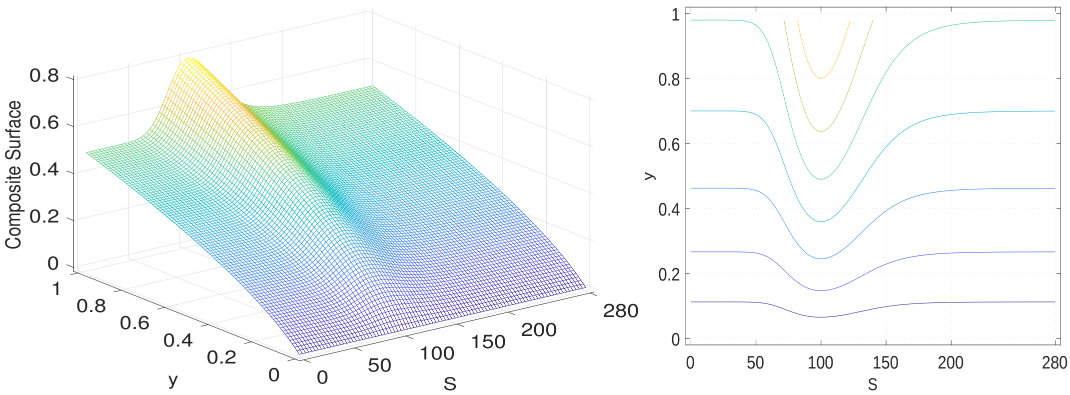

Figure 9. LEFT: A composite surface plot of $z_1(S)z_2(y)$; RIGHT: Corresponding contour map

Preprints (www.preprints.org) | NOT PEER-REVIEWED | Posted: 29 October 2018 doi:10.20944/preprints201810.0649.v1

Peer-reviewed version available at Algorithms 2019, 12, 30; doi:10.3390/a12020030

Now, we consider simulations over nonuniform spacial grids. To better design our tests, we are particularly interested in the following nonlinear distribution governing functions

$$\begin{aligned} z_1(S) &= \sqrt{\frac{1}{2.56} + \frac{25(S/100)^{10}}{2.56[1+(S/100)^5]^4}}, \quad S_{\min} \le S \le S_{\max}, \\ z_2(y) &= \frac{10\sqrt{0.5y}}{7}, \quad y_{\min} \le y \le y_{\max}, \end{aligned}$$

since they asymptotically fit into profiles of our option solution v as shown in experiments associated with uniform spacial meshes. Our nonuniform grids are generated via an arc-length equal-distribution principal for functions z_1, z_2 in S- and y-directions, respectively. The principal is commonly utilized in adaptive computations and serves as an initial exploration for more sophisticated adaptations [3,20]. The calculation of the mesh coordinates in our experiments is conducted based on a forward Euler formula for arc-lengths [18]. For instance, in the S-direction we have

$$S_{j+1} = S_j + \frac{\ell}{(N-1)\sqrt{1+[(z_1(S_j))_S]^2}}, \quad j = 1, 2, \ldots N-1,$$

where ℓ is the total arc-length, that is,

$$\ell = \int_{S_{\min}}^{S_{\max}} \sqrt{1+[(z_1(S))_S]^2}\, dS.$$

While the distribution functions z_1, z_2 are shown in Figure 8, their composite surface plots can be found in Figure 9. The latter characterizes the 2-dimensional profile of our grids distribution. The numerical solution acquired over such nonuniform grids, with $\rho = -0.5$ at $T = 0.5$ is given in Figure **??**.

3. Discussion

A dynamically balanced up-downwind semi-discretized finite difference method is constructed and analyzed in this paper based on arbitrary spacial grids. The algorithm acquired is easy to use. It is also effective for solving underlying Heston stochastic volatility option pricing model problems with cross-derivative terms. The scheme is proven to be numerically stable. The numerical method is expected to be first order in space. Computational experiments are carried out to verify our expectations both on uniform and nonuniform grids.

The spectral norm is used throughout this paper. The study can be extended by using different Euclidean norms. Our ongoing research has been including effective schemes on variable spacial and temporal meshes for different financial products and simulations. We have also been considering effective adaptation strategies such as those investigated in [16,18].

Our future endeavors also include improving the computational efficiency through exponential splitting methods, particularly variable step LOD approximations [3,8,20]. Compact schemes for raising the accuracy have also been introduced in our study with initial successes in handling cross-derivatives dynamically and well balances for pricing American and some Asian options [1,7,12,22].

Author Contributions: Conceptualization, C.S. and Q.S.; Methodology, C.S. and Q.S.; Software, C.S.; Validation, C.S. and Q.S.; Formal Analysis, C.S. and Q.S.; Investigation, C.S. and Q.S.; Resources, C.S. and Q.S.;Writing—Original Draft Preparation, C.S.; Writing—Review & Editing, C.S. and Q.S.; Visualization, C.S. and Q.S.; Supervision, Q.S.; Project Administration, C.S. and Q.S.; Funding Acquisition, Q.S.

Funding: This research work is partially supported by American Mathematical Society (Fan Research Award: AMS-F-32180177).

Acknowledgments: We are grateful to colleagues for their valuable and helpful discussions.

Conflicts of Interest: The authors declare no conflict of interest.

References

1. Albrecher H.; Predota M. On Asian option pricing for NIG Lévy processes. *J. Comp. Appl. Math.* **2004**, *172* ,153–168.
2. Black F.; Scholes M. The pricing of options and corporate liabilities. *J. Political. Econ.* **1973**, *81*, 637–654.
3. Cheng, H.; Lin P.; Sheng Q.; Tan R. Solving degenerate reaction-diffusion equations via variable step Peaceman-Rachford splitting. *SIAM J. Sci. Comput.*, **2003**, *25*, 1273–1292.
4. Düring B.; Fournié M. High-order compact finite difference scheme for option pricing in stochastic volatility models. *J. Comput. Appl. Math.* **2012**, *236*, 4462–4473.
5. Düring B.; Fournié M.; Heuer C. High-order compact finite difference schemes for option pricing in stochastic volatility models on non-uniform grids. *J. Comput. Appl. Math.* **2014**, *271*, 247–266.
6. Fornberg B. Calculation of weights in finite difference formulas. *SIAM Rev.* **1998**, *40*, 685–691.
7. Fusai G.; Meucci A. Pricing discretely monitored Asian options under Lévy processes. *J. Banking Finance.* **2008**, *32*, 2076–2088.
8. Hendricks C.; Ehrhardt M.; Günther M. High-order ADI schemes for diffusion equations with mixed derivatives in the combination technique.*Appl. Numer. Math.* **2016**, *101*, 36–52.
9. Heston S. A Closed-form for options with stochastic volatility with applications to bond and currency options. *Rev. Finan. Stud.* **1993**, *6*, 327–343.
10. K. J. in' t Hout; Welfert B. D. Stability of ADI schemes applied to convection-diffusion equations with mixed derivative terms. *Appl. Numer. Math.* **2007**, *57*, 19–36.
11. Hull J. C. *Option, futures and other derivatives*, 9th ed.; Pearson Education: New Jersey, USA, 2015.
12. Ikonen S.; Toivanen J. Efficient numerical methods for pricing American options under stochastic volatility. *Numer. Meth. PDEs.* **2008**, *24*, 104–126.
13. Iserles A. *A First Course in the Numerical Analysis of Differential Equations*, 2nd ed.; Cambridge University Press: New York, USA, 2008.
14. Lax P. D.; Richtmyer R. D. Survey of the stability of linear finite difference equations. *Comm. Pure Appl. Math.* **1956**, *9*, 267–293.
15. Ma K.; Forsyth P. A. An unconditionally monotone numerical scheme for the two-factor uncertain volatility model. *IMA J. Numer. Anal.* **2017**, *37*, 905–944.
16. Meng Q. J.; Ding D.; Sheng Q. Preconditioned iterative methods for fractional diffusion models in finance, *Numer. Meth. PDEs.* **2015**, *31*, 1382–1395.
17. Noble J.; Daniel J. W. *Applied Linear Algebra*, 3rd ed.; Prentice-Hall: New Jersey, USA, 1988.

18. Padgett J.; Sheng Q. Numerical solution of degenerate stochastic Kawarada equations via a semi-discretized approach. *Appl. Math. Comp.* **2018**, *325*, 210–226.
19. Rachev S. T. *Handbook of Computational and Numerical Methods in Finance*; Birkhäuser: Boston, USA, 2014.
20. Sheng Q.; Padgett J. On the stability of a variable step exponential splitting method for solving multidimensional quenching-combustion equations. *Springer Proc. Math. Stat.* **2016**, *171*, 155–167.
21. Shreve S. *Stochastic Calculus for Finance II: Continuous-Time Models*; Springer: New York, USA, 2004.
22. Zhu S. P.; Chen W. T. A predictor-corrector scheme based ADI method for pricing American puts with stochastic volatility. *Comput. Math. Appl.* (2011), *62*, 1–26.